Proceedings World Geothermal Congress 2020+1
Reykjavik, Iceland, April - October 2021

Seismicity Observed during the Development of the Rittershoffen Deep Geothermal Field (France)

Emmanuel Gaucher[1], Vincent Maurer[2], Marc Grunberg[3], Rike Koepke[1], Romain Pestourie[3], Nicolas Cuenot[2]

[1] KIT, Institute of Applied Geosciences, Division of Geothermal Research, Kaiserstraße 12, D-76131 Karlsruhe, Germany

[2] ES-Geothermie, 5 rue de Lisbonne, Le Belem, F-67300 Schilitigheim, France

[3] EOST, 5 rue René Descartes, F-67084 Strasbourg Cedex, France

emmanuel.gaucher@kit.edu

Keywords: Monitoring, Seismicity, EGS, Stimulation, Upper Rhine Graben.

ABSTRACT

The Rittershoffen deep geothermal plant, which is located 6 km east of Soultz-sous-Forêts (France), is operated since mid-2016 by the ECOGI joint venture. It is the youngest deep geothermal site exploited in the Upper Rhine Graben, several are currently under development in this area. The reservoir produces hot water at 170°C and delivers 24 MWth to a bio-refinery located 15 km away.

This field was developed from 2012 to 2016. The first well of the doublet (GRT-1) was completed end of 2012 and reaches the crystalline fractured basement which constitutes the reservoir formation together with the overlaying Buntsandstein sandstones. A reservoir development strategy was defined, and first consisted in enhancing the connections between GRT-1 and the fractured reservoir. These operations were applied in two sequences, respectively in April 2013, with a "thermal" stimulation and in June 2013, with a "hydraulic" stimulation. Both sequences generated seismicity that was not felt by the local population, the maximum magnitude reached 1.6 Mlv. The stimulations were successful, providing the expected enhancement of the hydraulic properties of the well. The drilling of the second well, GRT-2, which ended in July 2014, was followed by a production test highlighting good well productivity and no stimulation was carried out.

We present here the seismicity which was detected and located at Rittershoffen until the end of the GRT-2 well drilling. This seismicity was acquired by a permanent seismic network and several additional temporary stations implemented over the period. Event detection was carried out by the SeisComp3 software adapted for local seismicity processing and tuned, a posteriori, to the seismicity recorded at Rittershoffen. Following the automatic detection, manual review and picking was carried out and location was performed in a 3D velocity model derived from active seismic and well logs. More than 1300 events constitute the so-called reference database. We present the time, space and magnitude characteristics of the induced seismicity and discuss them in parallel with the operational parameters in order to better understand the reservoir behavior and the well doublet system at depth.

1. INTRODUCTION

The Upper Rhine Graben is a main target for geothermal exploitation of deep fractured formations in continental Europe. On the one hand, this is due to favourable temperature gradients encountered at relatively shallow depth: 60°C/km (Baillieux *et al.* 2013). On the other hand, extensive scientific and technical studies, initiated 30 years ago at the research pilot site of Soultz-sous-Forêts, contributed substantially to the better understanding of the processes occurring at depth and to the development of the Enhanced Geothermal Systems (EGS) concept (Genter *et al.* 2010). Hence, in the last decade, geothermal exploitation activity in the Upper Rhine Graben has been on going with several German and French sites such as Landau, Insheim, Bruchsal, Soultz-sous-Forêts and more recently Rittershoffen (Baujard *et al.* 2017). All of these projects exploit the deep fractured reservoirs located within Triassic-sediments and/or the crystalline basement. Currently, two sites are in active development in the Strasbourg area (France) and several are planned or in exploration phase.

The EGS technology consists in increasing the low natural hydraulic performance of geothermal fractured reservoirs by thermal, chemical and/or hydraulic stimulations. These stimulations increase the fracture permeability to allow producing (or reinjecting) the geothermal brine at economically viable flowrates. This is often accompanied by induced seismicity (Evans *et al.* 2012), which, on the one hand, must be controlled and mitigated (Gaucher *et al.* 2015) and, on the other hand, can be used to image the geothermal reservoir (Sausse *et al.* 2010). Here, we describe the main characteristics of the seismicity detected during the development of the Rittershoffen deep reservoir. This work follows the preliminary work presented by Maurer *et al.* (2015) and complement the work of Baujard *et al.* (2017) and Lengliné, Boubacar and Schmittbuhl (2017).

2. RITTERSHOFFEN CONTEXT

2.1 Geological Context

The deep geothermal field of Rittershoffen is located on the western margin of the NE–SW-striking central segment of the Upper Rhine Graben (URG) (Figure 1). The URG is a 300 km long, 40 km wide rift zone with an azimuthal extension averaging N20°E between Mainz and Bale (Ziegler *et al.* 2006). It is associated to the Rhine valley, which is structurally bounded in the South by the folded Jura, in the West by low relief Vosges mountain range, in the East by the Black Forest massif and in the North by the Vogelsberg volcanic massif.

Tectonically, the western and the eastern edge of the URG are limited by major normal faults. A regional extension started 40 My ago, which is at the origin of the spacing between the Occidental and Oriental Rhine faults. The sedimentological filling of the basin is syn-tectonic and affected by numerous normal faults resulting from the opening system while the extension was

accommodated by a series of normal faults in the sedimentary cover in the center of the graben. Stratigraphically, the uppermost part of the Rhine Graben is composed by Plio-Quaternary deposits, which uncomfortably cover Eocene and Oligocene formations whose deposition began during the regional extensional context. In the Mesozoic era, lack of Cretaceous sequence is observed in the URG due to a late Jurassic bulge phase, resulting in a 125 My hiatus in the depositional sequence. The Mesozoic and Paleozoic formations, in continuity with the Paris Basin, are exhumed at the rift flanks but buried, below the Tertiary cover, deeper in the center of the graben by tilted blocks. The Variscan crystalline basement is mainly composed of granites and granodiorites which have been set up 320-330 My ago.

2.2 Field Development

Rittershoffen geothermal reservoir is developed at the interface between the clastic Triassic sandstones and the top crystalline basement and targets local normal faults. The first well, GRT-1, reached a final depth of 2580 m end of the year 2012. Various logs and hydraulic tests were performed over the year 2013. As the well injectivity index was too low for economic exploitation, well-reservoir stimulation was carried out. These operations consisted in a thermal stimulation (April 2013) followed by a chemical and hydraulic stimulation (June 2013), which finally improved the injectivity index by a factor of 5 (Baujard *et al.* 2017). Then, after an active 2D seismic campaign, the second well, GRT-2, was drilled and completed in August 2014. The following production and circulation tests reached the expectations that prevented to stimulate GRT-2. A tracer test was also performed after the production test (October 2014). The year 2015 was dedicated to the building of a secondary loop to transport the heat to the bio-refinery located 15 km away, and to the building of the geothermal plant, which was commissioned in May 2016. The plant is operating since then. Before, during and after drilling operations, induced seismicity was monitored by a series of sensors.

3. SEISMIC MONITORING

3.1 Monitoring Networks

Six months prior to any drilling operation at Rittershoffen, a permanent monitoring network was installed in the area as required by legal authorities. This network consists of five short-period seismometers of three-components, which are installed on surface. It is connected to the "École et Observatoire des Sciences de la Terre" (EOST) of Strasbourg (University of Strasbourg) and send the continuous seismic data to a SeisComp3 server for automatic storage and processing. With the nearby Soultz-sous-Forêts EGS, seven other permanent surface stations are available and connected to the same system. This increases the coverage of the permanent monitoring.

With the development of the Rittershoffen reservoir, KIT proposed to install temporary three-component short-periods stations at surface to complete the existing network coverage (Gaucher *et al.* 2013; Gaucher, Maurer and Grunberg 2018). This was carried out stepwise in cooperation with ES-Géothermie and EOST. Hence, five additional stations were recording in June 2013 during the chemical and hydraulic stimulation of GRT-1 and 26 more prior to the drilling of GRT-2. The final temporary and permanent monitoring network was covering an area of at least 5 km radius around the well pad (Figure 1).

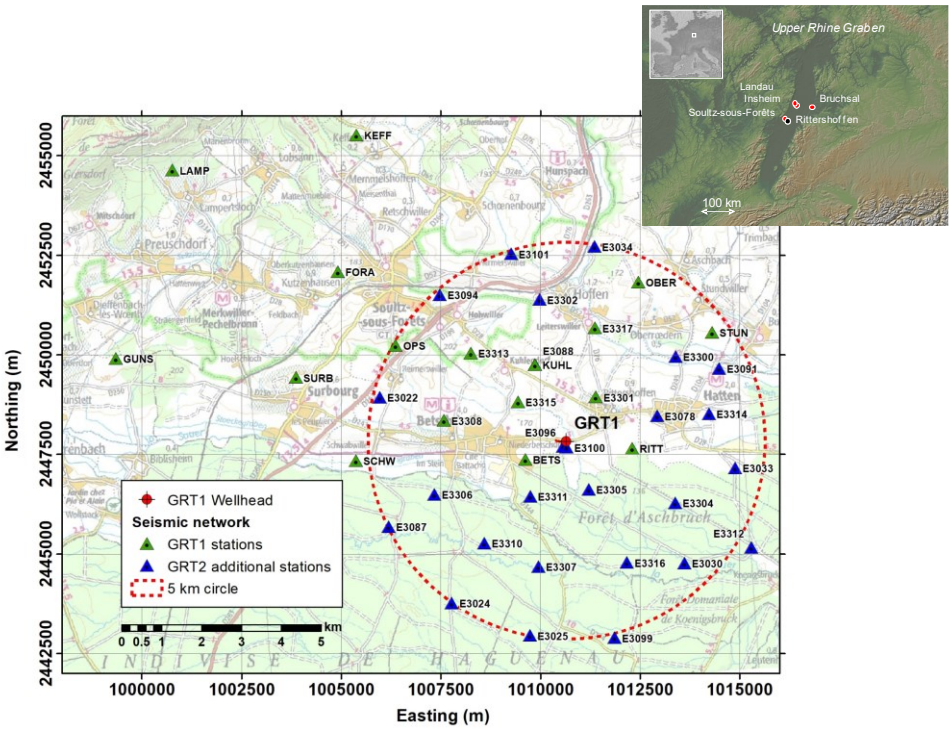

Figure 1: Seismic monitoring network around Rittershoffen. In green triangles are shown the stations monitoring during the chemical and hydraulic stimulation of GRT-1. They were completed before the drilling of GRT-2 by the stations shown as blue triangles. The temporary stations start with the letter "E".

3.2 Seismic Processing

The real-time monitoring of the field operations was associated with real-time automatic processing based on the SeisComp3 capabilities. As data were acquired, processed and analyzed, improvement of the automatic processing parameters occurred, in particular regarding the detection capabilities. This led to inhomogeneous detection capabilities over time until the automatic system took its final set-up. To find the optimum set of parameters, an operator manually reviewed the first six hours of data associated with the hydraulic stimulation. Then, tuning of the detection parameters was performed and, with the final set, a recovery rate of 96% of the reference database could be reached by the automatic system. This optimal automatic system was applied, a posteriori, on the continuous data recorded by all available stations, from the drilling of GRT-1 to the end of the drilling of GRT-2. This reprocessing stage guarantees homogeneous detection capabilities over our period of interest.

Following automatic detection and picking, all event candidates were manually reviewed and validated. The P- and S-wave picks were checked and corrected when necessary and the P-wave amplitude on the vertical component was measured for later local magnitude estimate. The location of the seismicity was done in a 3D velocity model. This 3D model was constructed in several steps. First, the interpretation of 2D seismic lines provided the main formation interfaces at depth. Then, the zero offset VSP acquired at GRT-1 was used to compute interval P-wave velocities for each identified formations and finally, a full-sonic log provided average Vp/Vs ratio per layer. This ratio was not available for the first 400 m below surface. To account, to a certain extent, for the sensitivity of the location to the S-wave velocity model and minimize effects from network coverage, the strongest events induced during the drilling of the GRT-2 well (see subsection 4.1) were located only with the P-waves and all time residuals, P and S, were used as stations corrections and systematically applied before locating all events (Maurer *et al.* Submit.). NonLinLoc software (Lomax *et al.* 2000; Lomax 2018) was used to locate the events. Following the location, a local magnitude of the events was estimated using the approach of Bakun and Joyner (1984) applied on the vertical components.

Assuming that the recorded seismicity, or a subset, follows a Gutenberg-Richter power law, we estimated the magnitude of completeness (M_C) and the corresponding b-value using the goodness-of-fit approach of Wiemer and Wyss (2000) in combination with a least-squares method.

4. RESULTS AND DISCUSSION

The application of the described processing procedure led to identify and locate 1348 earthquakes induced during GRT-1 drilling, thermal stimulation and hydraulic stimulation, and during GRT-2 drilling. The hydraulic stimulation of GRT-1 was the most seismogenic operation and account for 74% of the identified seismicity. This reference catalogue is available as supplementary material in Maurer *et al.* (Submit.)

The local magnitude of the seismicity ranged between -1.5 and 1.6. None of the induced event was felt by the population.

4.1 Seismicity during drilling

During drilling of GRT-1 and GRT-2 wells, seismicity was induced and linked to circulation losses. In both cases, this happened in the middle Muschelkalk formation (~ 1650 m TVD GL). In GRT-1 case, 26 seismic events, with magnitudes between -1.3 and 0.6, were identified within 30 min. In GRT-2 case, 184 earthquakes were identified in a 4-hour period, most of them occurring within one hour. Their magnitude ranged between -1.5 and 1.0 and the largest events were seen by almost all (41) stations of the network. Since the depth of the mud losses was known, these large events were also used to “calibrate” the velocity model (see subsection 3.2). Interestingly, the seismicity induced during GRT-2 drilling spread northward and southward from the well.

Assuming a Gutenberg-Richter power law distribution of the seismicity induced during the GRT-2 drilling, a b-value of 1.04 ± 0.02 was estimated, with a corresponding M_C of -0.75. Such a b-value is typical of tectonic context and is consistent with the reactivation of an existing fault.

4.2 Seismicity during GRT-1 thermal circulation

In April 2013, GRT-1 thermal stimulation was carried out and seismicity induced: 146 earthquakes, with magnitudes ranging from -1.5 to 0.3, have been detected and located during this ~2.5-days injection. Geothermal water (cooled down to about 10°C) was injected in the open-hole section of the well (sandstone and granite). Initially, the flow rate was 10 L/s and then increased to 15, 20 and 25 L/s, and before shut-in decreased to 20 and 15 L/s. A total of 4135 m³ were injected. The wellhead pressure (WHP) quickly increased to 2.8 MPa, at 15 L/s, and then always remained below that level, but generally above 1.8 MPa (Baujard *et al.* 2017).

The first event was detected 26 h after start of injection and 21 h after the largest WHP of 2.8 MPa was reached Figure 2. This observation may indicate that uncritically stressed zones connected to the open-hole existed or that rock cohesion was not negligible. The majority of the activity occurred when the flow rate reached 20 L/ and then 25 L/s, with a maximum rate close to one event per minute. Interestingly, the seismic rate decreased strongly while the injection rate was at 25 L/s but the WHP was decreasing from 2.7 to 2.0 MPa and such a behavior may have happened also earlier when the injection rate was at 20 L/s and the WHP was decreasing from 2.7 to 2.2 MPa. This suggests that an increase of injectivity generates less seismic events and that pressure and flow rate should always be considered together and not separately. The detected seismicity ended 11 h before decrease of the injection rate from 25 L/s to 20 L/s and when the WHP had decreased below 2 MPa.

As shown Figure 3, most of the earthquakes are clustered around and north of the GRT-1 well. Without considering outlier events, the remaining ones are oriented N3°E and are dipping 86°W. The cloud is ~1500 m long and ~500 m wide. Eighty percent of the hypocenters are between 1300 and 3050 m depth. The events in the north are the shallowest ones and those close to GRT-1 well, the deepest ones.

The b-value associated with the seismicity induced during thermal stimulation was estimated to 1.62 ± 0.04 with $M_C = -0.7$. This relatively high b-value is not inconsistent with other values observed for injection-induced seismicity (Cuenot, Dorbath and

Dorbath 2008; Dorbath *et al.* 2009; Bachmann *et al.* 2011). This can be interpreted as the creation or reopening of small cracks and fractures in the rock mass due to high stress variation near the injection interval, as expected from a thermal stimulation (Scholz 1968; El-Isa and Eaton 2014; Zang *et al.* 2014).

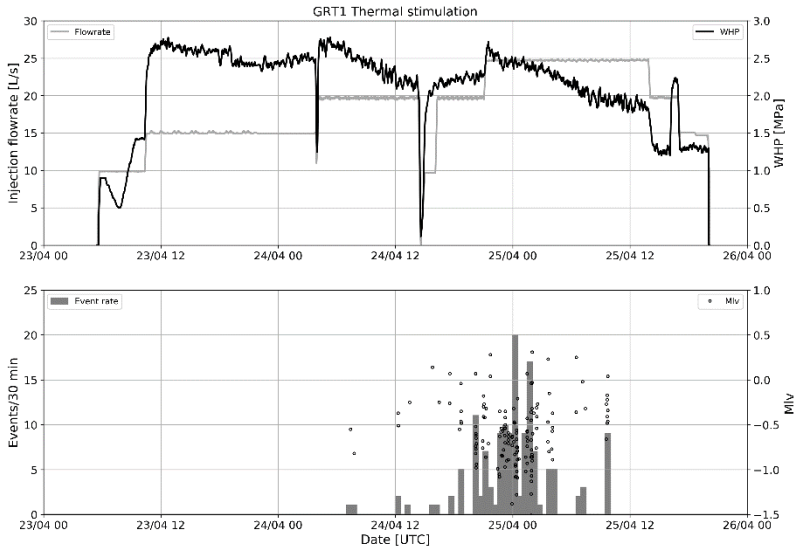

Figure 2: Occurrence of the seismicity recorded during GRT-1 thermal stimulation in parallel with the injection parameters. Top: injection flow rate (gray) and WHP (black); bottom: seismic rate per 30 minutes (gray bars) and event local magnitude (black circles).

4.3. Seismicity during GRT-1 chemical and hydraulic stimulation

In June 2013, a series of stimulations were performed in GRT-1: a pre-stimulation test (22/06), three chemical treatments for three isolated depth intervals of the open-hole (23, 24 and 25/06) and a hydraulic stimulation in the open-hole (27 and 28/06). This was followed by a short injection test (28/06) (Baujard *et al.* 2017). No seismic activity was detected during the pre-stimulation test and the chemical stimulations. This may be due to the small amount of injected fluids, less than 650 m³, but also to the rock stress memory effect (or Kaiser effect), which means that repeated loading of a rock mass generates seismicity only when and where maximum stress previously experienced is exceeded. Yet, the WHP and flow rates for these operations never exceeded those of the thermal stimulation.

Nonetheless, the hydraulic stimulation induced seismicity (Figure 4). This 22-hours fluid injection consisted in a stepwise increase of the flow rate from 5 to 80 L/s and then a stepwise decrease. Approximately 3180 m³ of brine were injected and 824 earthquakes were identified during the stimulation. The activity started after 6 hours of injection, when the flow rate and WHP reached 40 L/s and 1.5 MPa respectively. Then, seismicity occurred continuously with an average rate between 40 and 60 events/hour. However, a decrease of the rate can be seen at the 40 L/s injection rate associated with a decrease of the WHP from ~2.2 MPa to 2.0 MPa. Hence, a similar behavior as observed during the thermal stimulation happened. The sudden increase of rate to 50 L/s increased the seismic rate again. When the stepdown injection at the end of the stimulation started, seismicity decreased definitely and stopped when the rate was back to 50 L/s and the WHP to 2.2 MPa, 2.5 hours before shut-in. No seismicity was detected during the following injection test, which is likely another evidence of the Kaiser effect.

The magnitude of the events observed during hydraulic stimulation ranged between -1.4 and 0.9, and the largest event occurred when the injection rate increased to its highest value, 80 L/s. The b-value of this sequence of events was estimated to 1.38 ± 0.03 with Mc = -0.7. The magnitude of completeness is comparable to that of the thermal stimulation and the b-value is also higher than one, but smaller than that of the thermal stimulation. Accordingly, thermal stimulation may have had larger volumetric effects than the hydraulic stimulation.

The earthquakes induced during the hydraulic stimulation are located around GRT 1 and to the North (Figure 3). The best plane fitting them is oriented N1°E and is dipping almost vertically (89°W). Hence, this plane is consistent with the plane depicted by the seismicity induced during thermal stimulation. The cloud is ~1800 m long and less than 500 m wide. Most of the hypocenters are located between 1200 and 2000 m depth. The deepest events are close to GRT-1 at the injection depth whereas the shallowest events are located further north.

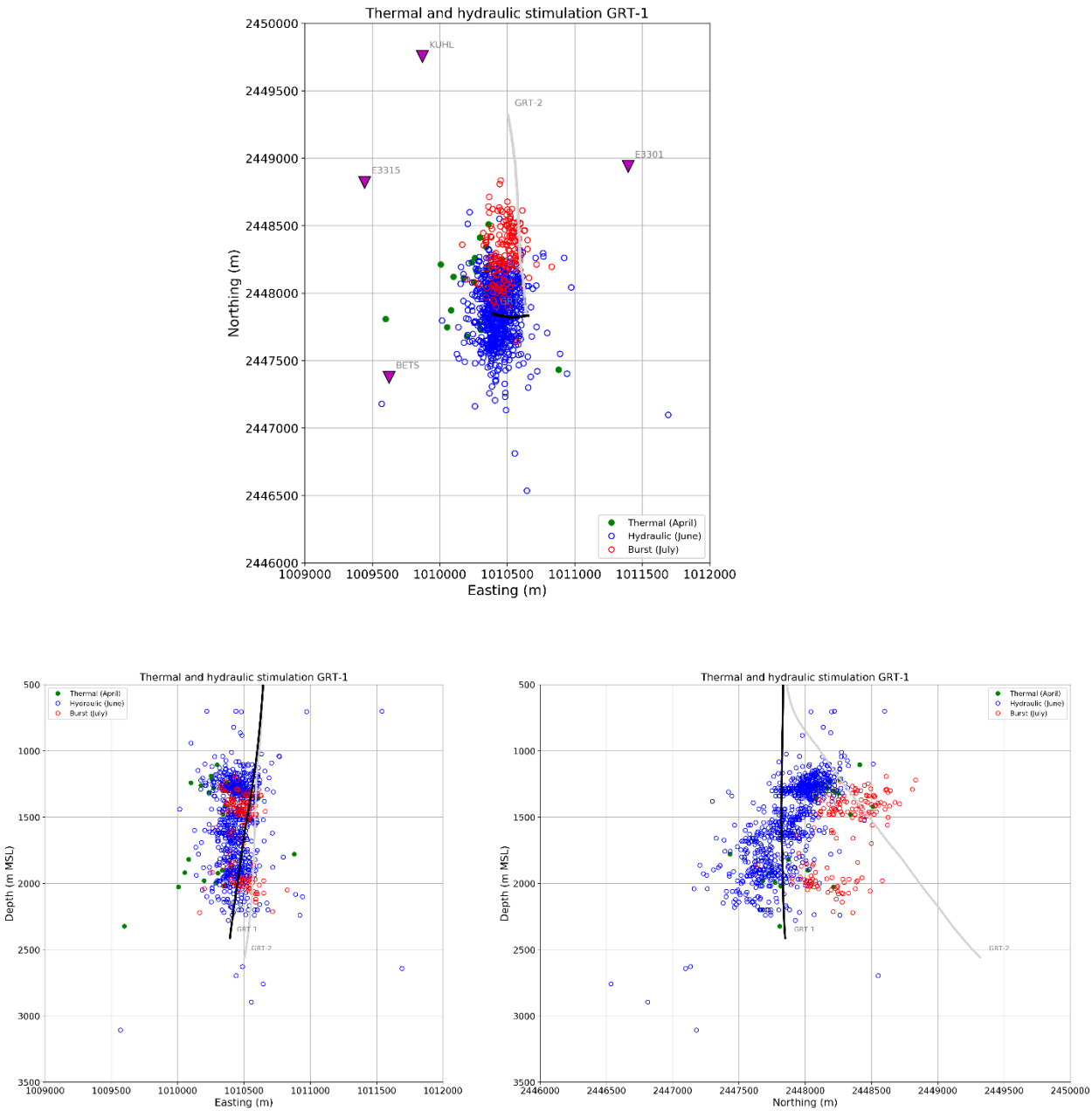

Figure 3: Location of the seismicity induced during thermal stimulation (green points), during hydraulic stimulation (blue circles) and after hydraulic stimulation, so-called "burst" of seismicity (red circles). Epicenter map (top), vertical EW projection (bottom left) and vertical NS projection (bottom right).

A striking observation associated with the hydraulic stimulation is the sudden burst of seismicity that occurred four days after injection, although no operation was made at the site (Figure 5). Within ~1.5 hours, 146 earthquakes with a magnitude between -0.9 and 1.6 were located. Among these events are the strongest ones recorded during the field development. Their b-value was estimated to 0.94 ± 0.02 with Mc = -0.2, which is in accordance with the reactivation of a major fault. This burst of seismicity is concentrated between 1300 and 1500 m, in the sedimentary layers and between 1900 and 2100 m, close to the basement-sediment interface (Figure 3). It extends further to the NNE the seismic cloud induced by hydraulic stimulation, which shows that stresses were already released in this zone and brings another evidence of the Kaiser effect. The latter could not be observe from the event hypocenters between the thermal stimulation and the hydraulic stimulation. We recall that the location method we applied is an absolute location method. Relative locations would certainly improve the relative positioning of all recorded events and then better image the structures, especially in depth. Kinnaert *et al.* (2016) showed that with the seismic network mainly located in the northern part of the area and the usual trade-off between depth and origin time determination of hypocenters from surface networks, the main direction of the location errors is approximately oriented to the south and dipping by about 45°. Such errors may be at the origin of the positioning of the events in the 1300 – 1500 m depth range, which is rather shallow and in the clay-rich Lias formation.

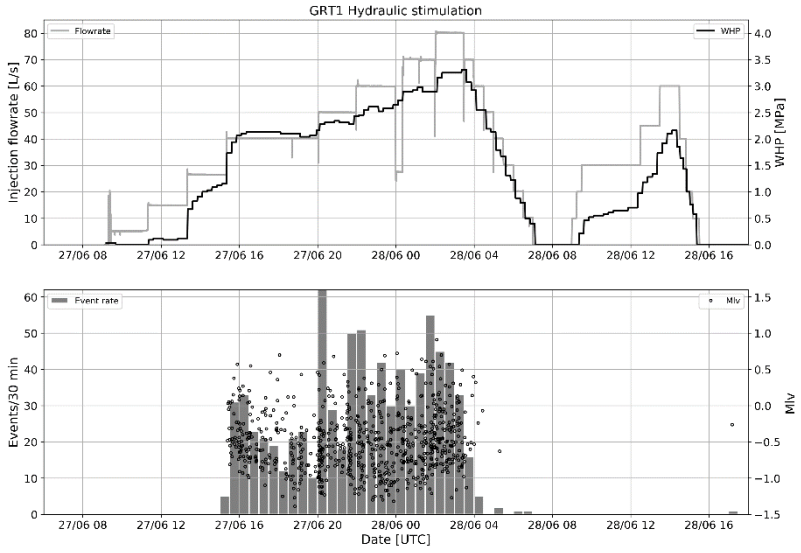

Figure 4: Occurrence of the seismicity recorded during GRT-1 hydraulic stimulation in parallel with the injection parameters. Top: injection flow rate (gray) and WHP (black); bottom: seismic rate per 30 minutes (gray bars) and event local magnitude (black circles).

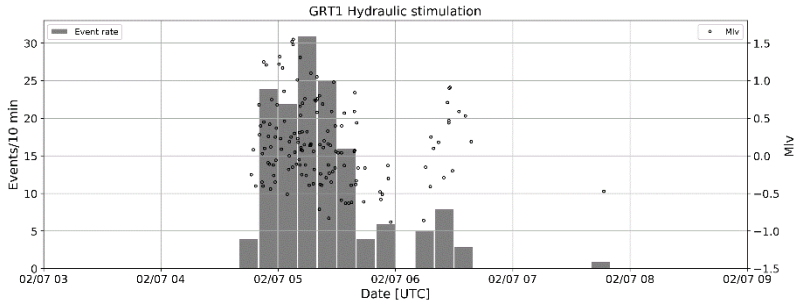

Figure 5: Occurrence of the burst of seismicity recorded four days after GRT-1 hydraulic stimulation: seismic rate per 10 minutes (gray bars) and event local magnitude (black circles).

5. CONCLUSION

More than 1300 micro-earthquakes were induced at Rittershoffen during the development of the geothermal reservoir. This seismicity with local magnitudes between -1.5 and 1.6 was not felt by the population. Most of the events, 85%, were directly or indirectly induced by the thermal and hydraulic stimulations of GRT-1, which involved about 4000 m³ of injected fluid each. The rest of the events were induced by mud losses in the Muschelkalk formation during drilling of both wells of the doublet.

The b-values of the different seismic sequences are consistent with the reactivation of existing faults for the seismicity associated with GRT-2 drilling and the burst of seismicity of July 2013, 4 days after hydraulic stimulation. For the latter, reactivation of the main Rittershoffen fault may be suspected, which is also supported by the larger magnitudes recorded in that period. During the injection periods, the creation and reopening of existing smaller structures is more likely, especially for the thermal stimulation.

A clear reduction of the seismic rate while injectivity was increasing has been observed during the thermal and hydraulic stimulations. Several evidences of the rock stress memory effect were also observed, especially the lack of seismicity recorded during the pre-stimulation test of GRT-1, during the chemical stimulations, for the first six hours of the hydraulic stimulation and during the final injection test. This Kaiser effect was however difficult to confirm from the event hypocenters except for the burst of seismicity, whose associated events were extended the previously seismogenic zone.

The seismicity is located almost vertically in an average N5°E direction. The Rittershoffen fault was likely reactivated at its intersection with GRT-1. The depth extension of the seismicity up to the clay-rich Lias formation is however questionable. This could be a trade-off between depth and origin time of the events due to the exclusive north coverage of the surface seismic network before GRT-2 drilling. Further investigations are however necessary before drawing any strong conclusion based on the seismic event hypocenters.

REFERENCES

Bachmann C.E., Wiemer S., Woessner J. and Hainzl S. 2011. Statistical analysis of the induced Basel 2006 earthquake sequence: introducing a probability-based monitoring approach for Enhanced Geothermal Systems. *Geophysical Journal International* **186** (2), 793–807.

Baillieux P., Schill E., Edel J.-B. and Mauri G. 2013. Localization of temperature anomalies in the Upper Rhine Graben: insights from geophysics and neotectonic activity. *International Geology Review* **55** (14), 1744–1762.

Bakun W.H. and Joyner W.B. 1984. The ML scale in central California. *Bulletin of the Seismological Society of America* **74** (5), 1827–1843.

Baujard C., Genter A., Dalmais E., Maurer V., Hehn R., Rosillette R., Vidal J. and Schmittbuhl J. 2017. Hydrothermal characterization of wells GRT-1 and GRT-2 in Rittershoffen, France: Implications on the understanding of natural flow systems in the rhine graben. *Geothermics* **65**, 255–268.

Cuenot N., Dorbath C. and Dorbath L. 2008. Analysis of the microseismicity induced by fluid injections at the EGS site of Soultz-sous-Forêts (Alsace, France): Implications for the characterization of the geothermal reservoir properties. *Pure and Applied Geophysics* **165** (5), 797–828.

Dorbath L., Cuenot N., Genter A. and Frogneux M. 2009. Seismic response of the fractured and faulted granite of Soultz-sous-Forêts (France) to 5 km deep massive water injections. *Geophysical Journal International* **177** (2), 653–675.

El-Isa Z.H. and Eaton D.W. 2014. Spatiotemporal variations in the b-value of earthquake magnitude–frequency distributions: Classification and causes. *Tectonophysics* **615-616**, 1–11.

Evans K.F., Zappone A., Kraft T., Deichmann N. and Moia F. 2012. A survey of the induced seismic responses to fluid injection in geothermal and CO2 reservoirs in Europe. *Geothermics* **41** (0), 30–54.

Gaucher E., Maurer V. and Grunberg M. 2018. *Temporary passive seismic data acquired at Rittershoffen geothermal field (Alsace, France, 2013-2014)*.

Gaucher E., Maurer V., Wodling H. and Grunberg M. 2013. Towards a dense passive seismic network over Rittershoffen geothermal field. In: *European Geothermal Workshop 2013b*, Strasbourg, France.

Gaucher E., Schoenball M., Heidbach O., Zang A., Fokker P.A., van Wees J.-D. and Kohl T. 2015. Induced seismicity in geothermal reservoirs: A review of forecasting approaches. *Renewable and Sustainable Energy Reviews* **52**, 1473–1490.

Genter A., Evans K., Cuenot N., Fritsch D. and Sanjuan B. 2010. Contribution of the exploration of deep crystalline fractured reservoir of Soultz to the knowledge of enhanced geothermal systems (EGS). *Comptes Rendus Geoscience* **342** (7-8), 502–516.

Kinnaert X., Gaucher E., Achauer U. and Kohl T. 2016. Modelling earthquake location errors at a reservoir scale: a case study in the Upper Rhine Graben. *Geophysical Journal International* **206**, 861–879.

Lengliné O., Boubacar M. and Schmittbuhl J. 2017. Seismicity related to the hydraulic stimulation of GRT1, Rittershoffen, France. *Geophysical Journal International* **208** (3), 1704–1715.

Lomax A. 2018. The NonLinLoc home page. Available at: http://alomax.free.fr/nlloc/.

Lomax A., Virieux J., Volant P. and Berge-Thierry C. 2000. Probabilistic Earthquake Location in 3D and Layered Models. In: *Advances in Seismic Event Location*, Vol. 18 (ed. C. Thurber and N. Rabinowitz), pp. 101–134. Springer Netherlands. ISBN 978-90-481-5498-2.

Maurer V., Cuenot N., Gaucher E., Grunberg M., Vergne J., Wodling H., Lehujeur M. and Schmittbuhl J. 2015. Seismic monitoring of the Rittershoffen EGS project (Alsace, France). In: *World Geothermal Congress 2015*, World Geothermal Congress, Melbourne, Australia. IGA.

Maurer V., Gaucher E., Grunberg M., Koepke R., Pestourie R. and Cuenot N. Submit. Seismicity induced during the development of the Rittershoffen geothermal field, France.

Sausse J., Dezayes C., Dorbath L., Genter A. and Place J. 2010. 3D model of fracture zones at Soultz-sous-Forêts based on geological data, image logs, induced microseismicity and vertical seismic profiles. *Comptes Rendus Geoscience* **342** (7-8), 531–545.

Scholz C.H. 1968. The frequency-magnitude relation of microfracturing in rock and its relation to earthquakes. *Bulletin of the Seismological Society of America* **58** (1), 399–415.

Wiemer S. and Wyss M. 2000. Minimum Magnitude of Completeness in Earthquake Catalogs: Examples from Alaska, the Western United States, and Japan. *Bulletin of the Seismological Society of America* **90** (4), 859–869.

Zang A., Oye V., Jousset P., Deichmann N., Gritto R., McGarr A., Majer E. and Bruhn D. 2014. Analysis of induced seismicity in geothermal reservoirs – An overview. *Geothermics* **52**, 6–21.

Ziegler P.A., Schumacher M.E., Dèzes P., van Wees J.-D. and Cloetingh S. 2006. Post-Variscan evolution of the lithosphere in the area of the European Cenozoic Rift System. *Geological Society, London, Memoirs* **32** (1), 97–112.

Acknowledgments

The authors thank the ECOGI joint venture for funding part of the monitoring network and for sharing data with the scientific community. We thank the Geophysical Instrument Pool Potsdam from the GFZ German Research Centre for Geosciences for providing the temporary seismological units deployed by KIT. The deployment of the temporary network received support and funds from the excellence laboratory "LabEx G-EAU-THERMIE PROFONDE" (University of Strasbourg) as part of the French "Investments for the future" of the French National Research Agency. We also thank H. Wodling, H. Jund and C. Schnell (from EOST) for their support in the deployment of the temporary seismic network, C. Baujard, A. Genter (from ESG) who shared their experience and knowledge about the field operations, J. Schmittbuhl and O. Lengliné (from EOST) for fruitful discussions and Nicolas Perrinel for his work on the 3D velocity model. We also would like to thank Gempa GmbH and the GFZ for providing and maintaining the SeisComp3 software. This work was also conducted in the frame of the DESTRESS project which received funding from the European Union's Horizon 2020 research and innovation program under grant agreement No 691728. The authors acknowledge the support of the French national research agency (ANR), under grant ANR-15-CE06-0014-04 (Cantare Alsace).